J. Fluid Mech. (1993), *vol.* 249, *pp.* 499–519

Large-amplitude interfacial waves on a linear shear flow in the presence of a current

By GEORGE BREYIANNIS[1], VASILIS BONTOZOGLOU[2], DIMITRIS VALOUGEORGIS[1] AND APOSTOLOS GOULAS[1]

[1] Laboratory of Fluid Mechanics and Turbomachinery, Department of Mechanical Engineering, Aristotle University of Thessaloniki, 54006 Thessaloniki, Greece

[2] Department of Mechanical Engineering, University of Thessaly, Pedion Areos, 38334 Volos, Greece

(Received 20 January 1992 and in revised form 23 September 1992)

The properties of two-dimensional steady periodic interfacial gravity waves between two fluids in relative motion and of constant vorticities and finite depths are investigated analytically and numerically. Particular attention is given to the effect of uniform vorticity, in the presence of a current velocity, on the two factors (identified in the literature as dynamical and geometrical limits) which limit the existence of steady gravity wave solutions. The dynamical limit to the existence of steady solutions is found to be significantly influenced by the uniform vorticity of the lower fluid. In particular, the effect of non-zero vorticity is qualitatively different between a very shallow and a relatively deep lower fluid. Profiles and flow fields corresponding to very steep waves are calculated for a wide range of parameter values. The effect of uniform vorticity on the interfacial wave structure is demonstrated through a direct comparison with irrotational waves. For negative vorticity and high current velocity, a new flow structure is found, consisting of a closed eddy attached to the interface below the crest. Resemblance with shallow water waves breaking under strong air flow, (described in the experimental literature as roll waves) is noted.

1. Introduction

Liquid layers sheared by cocurrent gas (or immiscible liquid) flow appear in a variety of process equipment as well as in natural flows. For slightly viscous fluids in turbulent flow, steep gradients in the velocity profiles form close to the interface and the situation can be modelled by uniform velocities with a discontinuity across the interface. Interfacial waves in this context have been studied by many investigators (Drazin 1970; Maslowe & Kelly 1970; Nayfeh & Saric 1972; Saffman & Yuen 1982; Pullin & Grimshaw 1983; Miles 1986; Bontozoglou & Hanratty 1988) with particular emphasis on nonlinear extension of the classical Kelvin–Helmholtz instability.

It is evident however that for sufficiently thin films or viscous liquids, vorticity will be distributed across the entire layer instead of being concentrated only close to the interface. In the limit of laminar flow the base solution (without waves) is a linear shear flow. Under these circumstances, a constant-vorticity liquid layer bounded by a gas in uniform irrotational flow, with a velocity discontinuity across the interface, seems a more appropriate model. This configuration could be realistic for some liquid/liquid flows as well, namely when the upper, lighter liquid has considerably smaller molecular viscosity than the lower, a representative example being the flow of water over a layer of heavy oil.

There is also evidence that the above approach could occasionally be useful even for gas–liquid flows with uneven vorticity distribution, in particular at the limits of short waves and waves long with respect to the liquid depth. In the former, the vorticity can satisfactorily be approximated by its local value, whereas in the latter it has been argued (Teles da Silva & Peregrine 1988) that it is the existence of a non-zero mean vorticity that is important, rather than its specific distribution.

The present work deals with two-dimensional, inviscid waves in the aforementioned, constant vorticity, configuration. (An inviscid approximation seems realistic since the velocity profile in the liquid is typically established over timescales which are long compared with the wave period.) In particular, the effect of constant vorticity on the two different factors, (identified by Saffman & Yuen 1982 as dynamical and geometrical limits) which limit the existence of steady gravity wave solutions is investigated. The geometrical limit is associated with an unphysical shape of the wave as the wave height increases, while the dynamical limit is associated with the well-known Kelvin–Helmholtz instability. Note that recent interest in the constant-vorticity approximation (Simmen & Saffman 1985; Teles da Silva & Peregrine 1988; Milinazzo & Saffman 1990) is limited to surface waves and, to the best of our knowledge, no results have been reported on interfacial waves in the presence of a current.

The waves are functions of the wave height $H(=2a)$, the ratio of fluid densities r, the magnitude of the velocity discontinuity (current velocity) U, the distance of the interface from the upper and lower boundaries and the vorticities of the two layers. The whole parameter space is not fully described in the numerical part of the present work. In most cases the upper boundary is taken to infinity and the vorticity of the upper fluid is taken equal to zero. However, the analytical dispersion relations are complete in the sense that vorticity and finite depth in both fluids are included. Emphasis is given to small values of the density ratio (gas/liquid flows) and to values of vorticity with sign consistent with a shear generated by the velocity discontinuity.

The formulation and a linear analysis of the problem is given in §2, followed by the development of a weakly nonlinear approximation and a numerical method in §§3 and 4 respectively. The main analytical and numerical results are presented and discussed in §§5.1 and 5.2. Finally, some new characteristics of the flow structure of constant-vorticity waves in the presence of high current velocities are presented in §6, followed by the conclusions of the work in §7.

2. Problem formulation and linear analysis

The flow configuration under consideration is sketched in figure 1, where both a physical reference frame and a reference frame with the wave at rest are shown. The interface is located at $y = \eta(x)$ while the top and bottom boundaries are at d_2 and $-d_1$ respectively. The origin is chosen so that the mean elevation $\overline{\eta(x)}$ over one wavelength is zero. Properties of the lower fluid are denoted by subscript 1 and those of the upper fluid by subscript 2. The two fluids are assumed to be stably stratified by gravity so $\rho_2 < \rho_1$, and the upper fluid is moving relative to the lower fluid with a horizontal velocity U. The undisturbed flow is a shear flow with a velocity that varies linearly in the vertical direction. The magnitude of the shear is specified by ζ_1 and ζ_2 for the lower and upper fluid respectively and the vorticities ζ_1 and ζ_2 are perpendicular to the (x, y)-plane. The flow is assumed incompressible and inviscid, therefore the shear is produced by external effects. In figure 1 (*a*) the flow for $\zeta_1 < 0$ is shown, with the wave propagating downstream. This flow configuration is equivalent to a shear flow generated by the wind. Figure 1 (*b*) shows the flow pattern for $\zeta_1 > 0$ and the

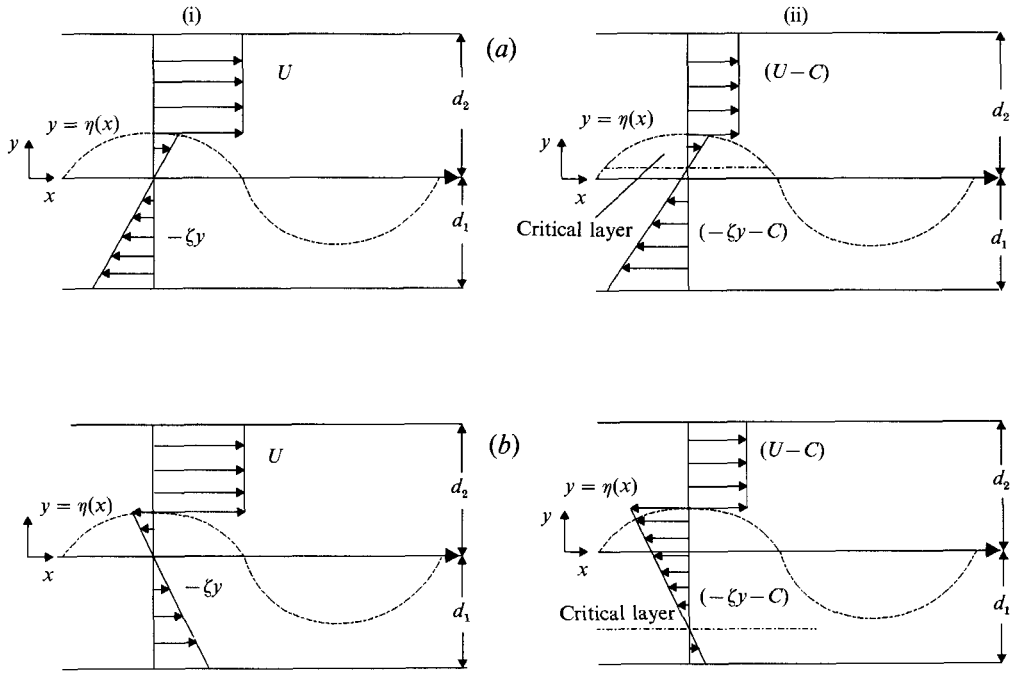

FIGURE 1. Sketch of the flow configuration. (*a*) Wave propagating downstream, $\zeta < 0$, (*b*) wave propagating upstream, $\zeta > 0$. (i) Physical reference frame, (ii) reference frame moving with the wave phase velocity.

corresponding upstream propagation. In figure 1 the vorticity of the upper fluid is taken equal to zero but in general can have either sign.

The vorticities remain uniform and constant throughout the two layers and in this case the fluid velocities can be written as

$$\boldsymbol{u}_1 = \left(\frac{\partial \phi_1}{\partial x} - \zeta_1 y, \frac{\partial \phi_1}{\partial y}\right) \tag{2.1}$$

and

$$\boldsymbol{u}_2 = \left(\frac{\partial \phi_2}{\partial x} - \zeta_2 y, \frac{\partial \phi_2}{\partial y}\right) \tag{2.2}$$

where the velocity potential function $\phi_i\, i = 1, 2$, satisfies Laplace equation $\nabla^2 \phi_i = 0$ in the entire fluid domain.

The kinematic boundary conditions that require the interface to move with the vertical velocity of the fluids are

$$\frac{\partial \eta}{\partial t} + \left(\frac{\partial \phi_i}{\partial x} - \zeta_i y\right)\frac{\partial \eta}{\partial x} = \frac{\partial \phi_i}{\partial y} \quad \text{at} \quad y = \eta, \quad i = 1, 2. \tag{2.3}$$

The dynamic boundary condition of equal pressures at the interface is expressed in a reference frame moving horizontally with C thus rendering the interfacial wave motionless. This will prove more convenient for the numerical computation. Using (2.1) and (2.2) the following is derived:

$$\tfrac{1}{2}\left[\left(\frac{\partial \phi_1}{\partial x} - \zeta_1 y - C\right)^2 + \left(\frac{\partial \phi_1}{\partial y}\right)^2\right] - \tfrac{1}{2} r\left[\left(\frac{\partial \phi_2}{\partial x} - \zeta_2 y - C\right)^2 + \left(\frac{\partial \phi_2}{\partial y}\right)^2\right] + (1-r) g\eta + K = 0, \tag{2.4}$$

where K is an unknown constant which is part of the solution. The no-penetration conditions at the top and bottom boundaries are

$$\partial\phi_i/\partial y = 0, \quad i = 1, 2. \tag{2.5}$$

A first insight in the characteristics of the waves with constant vorticity may be obtained through linear analysis. The linearized solution of the problem is readily found and gives a dispersion relation which can be written as

$$\frac{1+x}{1-x}C^2 + r\frac{1+y}{1-y}(U-C)^2 = \frac{g}{k}(1-r) + \frac{C}{k}\zeta_1 + r\frac{U-C}{k}\zeta_2, \tag{2.6}$$

where $x = \exp(-2kd_1)$, $y = \exp(-2kd_2)$, g is the gravitational acceleration, k is the wavenumber and r is the density ratio ρ_2/ρ_1. Solving the algebraic quadratic equation (2.6) for the linear wave speed C and taking for simplicity $\zeta_2 = 0$ gives

$$C = u_d + \frac{rY(U-u_d)}{X+rY} \pm \left[\left(C_0^2 + \frac{Xu_d^2}{X+rY}\right) - \frac{rXY}{(X+rY)^2}(U-u_d)^2\right]^{\frac{1}{2}}, \tag{2.7}$$

where

$$X = \frac{1+x}{1-x}, \quad Y = \frac{1+y}{1-y} \tag{2.8}$$

and

$$C_0^2 = (g/k)(1-r)/(X+rY) \tag{2.9}$$

is the dispersion relation for linearized irrotational waves in the absence of steady flow U. Finally,

$$u_d = \zeta_1/2kX \tag{2.10}$$

is the velocity of the liquid basic flow at a depth $W = 1/2kX$ below the interface. In the case of surface waves ($r = 0$) with shear, the dispersion relation has been interpreted (Teles da Silva & Peregrine 1988) as showing that the waves travel symmetrically with respect to the flow at a depth W. In the present context, (2.7) indicates that the Kelvin–Helmholtz model with shear is similar to an irrotational system where the lower fluid moves with a uniform velocity u_d. The analogy is not exact, since the term $[C_0^2 + Xu_d^2/(X+rY)]$ is always greater than the linearized irrotational phase speed. Therefore, non-zero vorticity has through this term a stabilizing effect, while $U-u_d < U$ only when $u_d > 0$. It is seen that positive vorticity linearly stabilizes the flow whereas negative vorticity could have either effect.

The critical linear current velocity reduces from (2.7) to

$$U_{cl} = u_d \pm \left[\frac{(X+rY)^2}{rXY}\left(C_0^2 + \frac{Xu_d^2}{X+rY}\right)\right]^{\frac{1}{2}}. \tag{2.11}$$

There is no loss of generality if only the positive root U_{cl}^+ is considered when both negative and positive vorticities are included. The negative root U_{cl}^- with $\zeta' = -\zeta$ corresponds to the same physical combination of shear and current, only in the negative x-direction. Differentiating equation (2.11) with respect to ζ, taking $\partial U_{cl}/\partial\zeta = 0$ and substituting the resulting expression for ζ_{min} back into (2.7), yields that $U_{cl_{min}}$ corresponds to $C = 0$. Then (2.6) yields directly

$$U_{cl_{min}} = C_0\left(\frac{X+rY}{rY}\right)^{\frac{1}{2}} \tag{2.12}$$

and
$$\zeta_{\min} = -2rYkU_{\mathrm{cl}_{\min}}. \tag{2.13}$$

It is observed that the linear critical current velocity U_{cl} is not a symmetric function of ζ with respect to the line $\zeta = 0$. Furthermore the minimum of U_{cl} is located in the region of negative vorticity.

3. Weakly nonlinear approximation

The characteristics of weakly nonlinear steady waves may be obtained by substituting Stokes expansions directly in the original set of equations and boundary conditions. This tedious algebraic manipulation is reduced when a variational principle approach is implemented.

The variational principle for rotational waves given by Bateman (1944) and Luke (1967) reduces to

$$\delta \int_R \int_{-d}^{\eta} \left[\frac{\partial \phi}{\partial t} + \tfrac{1}{2}(\nabla\phi - \zeta y)^2 + gy\right] \mathrm{d}y\,\mathrm{d}x\,\mathrm{d}t \tag{3.1}$$

for the case of two-dimensional inviscid waves with constant vorticity. In (3.1) ϕ is the velocity potential of the irrotational flow, ζ denotes the constant vorticity, $\eta(x, t)$ is the surface profile, y is the vertical coordinate and R is an arbitrary region in the (x, t) space. The similarity of the above principle with the variational principle given by Whitham (1974) and implemented by Saffman & Yuen (1982) and Bontozoglou & Hanratty (1988) to study irrotational two-dimensional waves, is evident. Following similar arguments the equivalence of the above principle with the equations and the boundary conditions describing free-surface inviscid flows with constant vorticity can be easily demonstrated. The Lagrangian for interfacial waves is the sum of the two single-layer expressions and may be defined as

$$L = -\overline{\int_{-d_1}^{\eta} \left[\frac{\partial \phi_1}{\partial t} + \tfrac{1}{2}(\nabla\phi_1 - \zeta_1 y)^2 + gy\right] \mathrm{d}y} - \overline{\int_{\eta}^{d_2} \left[r\frac{\partial \phi_2}{\partial t} + \tfrac{1}{2}r(\nabla\phi_2 - \zeta_2 y)^2 + rgy\right] \mathrm{d}y}, \tag{3.2}$$

where the overbar denotes integration over one wavelength. Manipulating (3.2), in a manner shown in the Appendix, the following second-order dispersion relation is obtained:

$$\begin{aligned}
&\frac{1+x}{1-x}C^2 + r\frac{1+y}{1-y}(U-C)^2 - \frac{g}{k}(1-r) - \frac{C}{k}\zeta_1 - r\frac{U-C}{k}\zeta_2 \\
&\quad = a^2\left[\tfrac{1}{2}k^2\left(\lambda^2\frac{1+x}{1-x} + r\lambda'^2\frac{1+y}{1-y}\right) - 2k^2\left(\lambda^2\frac{1+x}{1-x}\frac{x}{(1-x)^2} + r\lambda'^2\frac{1+y}{1-y}\frac{y}{(1-y)^2}\right)\right. \\
&\qquad -\frac{1}{4}\left(\zeta_1^2\frac{1+x^2}{1-x^2} + r\zeta_2^2\frac{1+y^2}{1-y^2}\right) + 2k\left(\lambda\zeta_1\frac{x}{(1-x)^2} + r\lambda'\zeta_2\frac{y}{(1-y)^2}\right) \\
&\qquad \left. + \tfrac{1}{2}k^2\frac{\left(\lambda^2\dfrac{1+4x+x^2}{(1-x)^2} - r\lambda'^2\dfrac{1+4y+y^2}{(1-y)^2} - \dfrac{2}{k}\left(\lambda\zeta_1\dfrac{1+x^2+x}{1-x^2} - r\lambda'\zeta_2\dfrac{1+y^2+y}{1-y^2}\right) + \dfrac{\zeta_1^2 - r\zeta_2^2}{2k^2}\right)^2}{\lambda^2\dfrac{1-x}{1+x} + r\lambda'^2\dfrac{1-y}{1+y}}\right],
\end{aligned} \tag{3.3}$$

where $\lambda = \omega/k$ is the linear rotational wave speed given by (2.7), $\lambda' = U - \lambda$, while the depth parameters x and y have been defined in §2. Equation (3.3) provides a second-order solution for the wave phase speed in terms of all parameters involved in the present formulation. The second-order dispersion relation (3.3) was originally derived by Pullin & Grimshaw (1986), in a slightly different context, as the interaction between the primary wave and its second harmonic.

For irrotational waves ($\zeta_1 = \zeta_2 = 0$) equation (3.3) reduces to the second-order dispersion relation of Bontozoglou & Hanratty (1988). Similar dispersion relations for rotational waves with constant vorticity have been presented in the literature for deep-water surface waves by Simmen & Saffman (1985) and for interfacial waves by Pullin & Grimshaw (1983). The present expression reduces to the existing dispersion relations by choosing the appropriate set of parameters.

4. Numerical method

The numerical method used is an extension of the one proposed by Bontozoglou & Hanratty (1988). An outline of the method is provided here for completeness, together with a detailed description of all necessary modifications. The reader is referred to the original publication for a more detailed exposition of the fundamentals.

4.1. *Outline*

The wave is characterized by its phase velocity C and the problem is solved in a coordinate system moving horizontally with velocity C. Equation (2.4) is applied at N points along the interface. These equations together with the specification of the mean wave elevation $\bar{\eta} = 0$ form an algebraic system of $N+1$ equations, with the profile elevations at N points and the combined Bernoulli constant K unknown.

The system is solved by a variation of Newton's method. At each iteration the fluids velocities at the interface are calculated by applying a boundary integral method for the known boundary (the outcome of the last iteration) moving horizontally with the known velocity C. The matrix of partial derivatives is calculated numerically by perturbing each elevation by a small amount and computing the change in velocity at each point. It was found to be both efficient and time-saving to calculate the matrix once and use these values for all iterations. Owing to the approximation introduced by substituting integrals with linear sums, the set of equations is not satisfied exactly. Instead, the mean-square error is minimized over N points. The criterion works satisfactorily in the sense that it is easily driven to a minimum, which decreases by increasing the discretization N.

4.2. *Boundary integral method*

The boundary integral formulation is the one developed by Longuet-Higgins & Cokelet (1976) and extended for finite depths by New, McIver & Peregrine (1985). It is used to calculate the irrotational part of the velocity field, while the rotational contribution is incorporated according to (2.1) and (2.2).

The transformation

$$z = r\,\mathrm{e}^{\mathrm{i}\theta} = \mathrm{e}^{\mp\mathrm{i}(x+\mathrm{i}y)}, \tag{4.1}$$

is applied (for the lower/upper fluid respectively), mapping one wavelength of the interface to a closed curve C_1 and the horizontal boundary $y = -d_1$ (or $y = d_2$) to a circle C_2 of radius $\exp(-d_1)$ (or $\exp(d_2)$ respectively). The transformed z-plane is shown in figure 2.

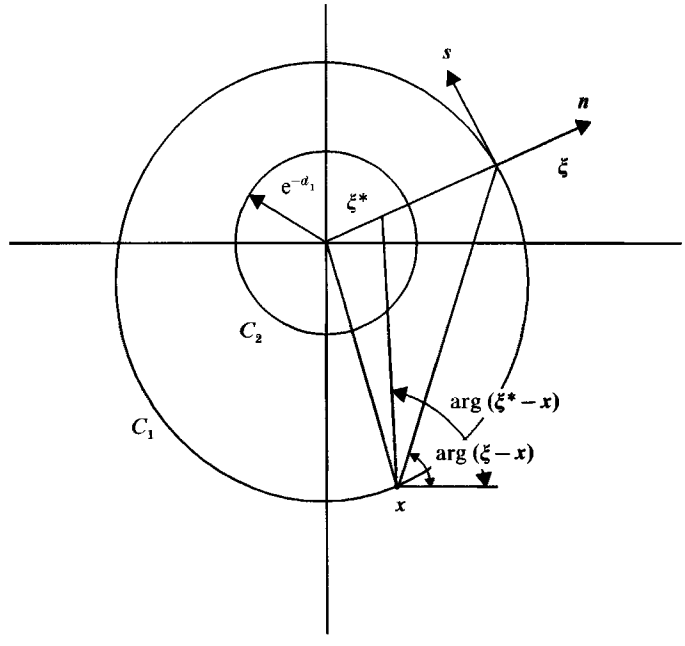

FIGURE 2. The transformed z-plane showing the construction of Green's function.

Suppose x is fixed at some point on the fluid boundary C_1 and ξ is allowed to vary along C_1. Let (s,n) be the tangential and normal coordinates at a point ξ on the boundary. Green's third identity is invoked using as Green's function

$$G(x;\xi) = \frac{1}{2\pi}\ln(|\xi - x|\,|\xi^* - x|) = \frac{1}{2\pi}\ln R(x;\xi), \tag{4.2}$$

with $\xi^* = e^{-2d}\xi/|\xi|^2$. By integrating along C_1 (the contribution from C_2 is identically zero) the following integrodifferential equation is derived:

$$\oint_{C_1} \ln R(x;\xi)\frac{\partial\phi}{\partial n}\,ds = -\oint a(x;\xi)\frac{\partial\phi}{\partial s}\,ds, \tag{4.3}$$

where $a(x;\xi) = \arg(\xi - x) - \arg(\xi^* - x)$ and the right-hand side is a principal-value integral. The essence of the method is that $\partial\phi/\partial n$ is known from the kinematic boundary conditions (2.3), and (4.3) can be discretized to calculate $\partial\phi/\partial s$ and subsequently the velocity magnitudes appearing in (2.4).

For waves of permanent form, the kinematic boundary conditions lead to

$$-C\frac{\partial\eta}{\partial x} + \frac{\partial\phi_i}{\partial x}\frac{\partial\eta}{\partial x} - \zeta_i y\frac{\partial\eta}{\partial x} = \frac{\partial\phi_i}{\partial y}, \quad i = 1,2. \tag{4.4}$$

If $N = (-\partial\eta/\partial x, 1)/[1 + (\partial\eta/\partial x)^2]^{\frac{1}{2}}$ is the unit normal to the interface, (4.4) becomes

$$\frac{\partial\phi}{\partial N} = -(C + \zeta_i y)\frac{\partial\eta}{\partial x}\Big/\left[1 + \left(\frac{\partial\eta}{\partial x}\right)^2\right]^{\frac{1}{2}}, \quad i = 1,2. \tag{4.5}$$

This is the correct boundary condition which needs also to be transformed to the z-plane before being used with (2.4).

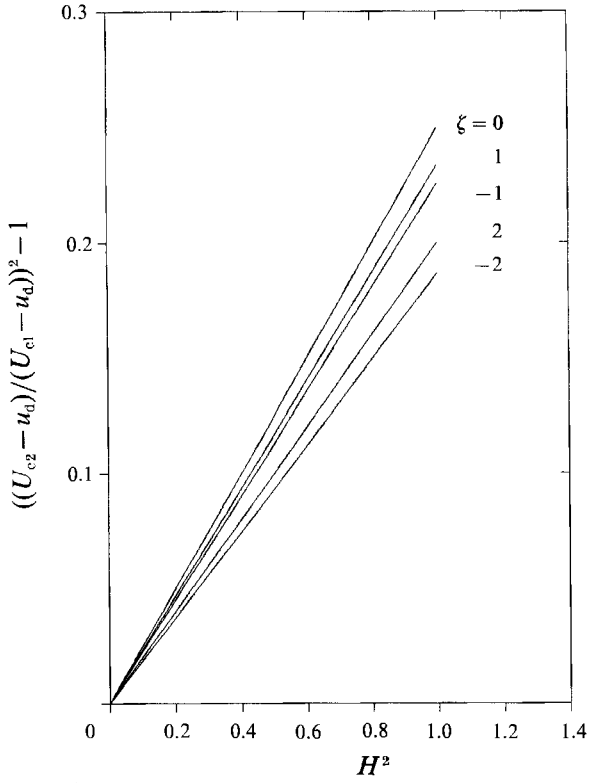

FIGURE 3. Critical current U_{c2} as a function of wave height H for density ratio $r = 0.001$, $\exp(-d_1) = 0.5$ and various vorticities ζ.

It is seen that by introducing a constant-vorticity model only a slight modification of the method proposed by Bontozoglou & Hanratty (1988) is required in order to obtain a numerical code for waves on a linear shear flow.

5. Results

The results presented are dimensionless quantities. All lengths are non-dimensionalized with the wavenumber k and the velocities are represented as Froude numbers using k^{-1} as characteristic length. All actual computations have been performed by taking the wavelength $L = 2\pi$ ($k = 1$), the lower fluid density $\rho_1 = 1$ and the gravitational acceleration $g = 1$.

5.1. *Analytical results*

It can be seen from (2.7) that for linear waves there are two solutions with different phase velocities C. These merge into one and subsequently disappear when U exceeds the critical value U_{c1} given by (2.11).

For finite-amplitude waves ($a \neq 0$) these two solutions continue into two families $C_+(a)$ and $C_-(a)$. From the form of the second-order dispersion relation (3.3) it can be seen that there will again be a critical current U_c beyond which steady solutions no longer exist. An increase in U_c with increasing wave amplitude has been viewed by Saffman & Yuen (1982) as a stabilization of parallel flows by waves. This is so because, for $U_{c1} < U < U_c$, steady linear waves do not exist whereas finite-amplitude ones are possible (whether these finite-amplitude waves are stable or not is a different question).

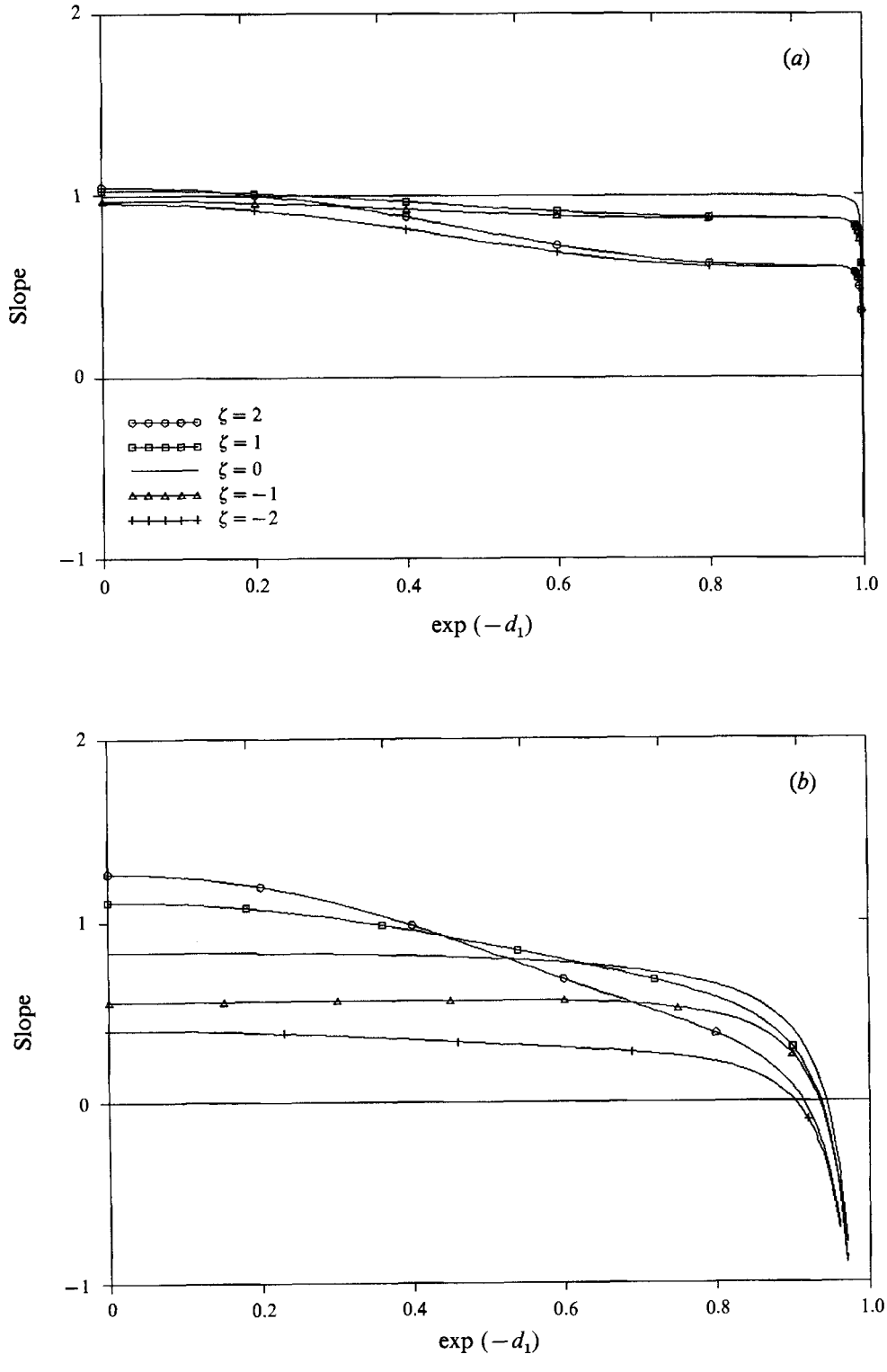

FIGURE 4. The slope of $((U_{c2}-u_d)/(U_{c1}-u_d))^2-1$ versus a^2, as a function of $\exp(-d_1)$ for various vorticities ζ and $\exp(-d_2) = 0$. (*a*) $r = 0.001$, (*b*) $r = 0.1$.

On the other hand, a decrease in U_c with increasing wave amplitude has been observed by Bontozoglou & Hanratty (1988) for very thin liquid films in irrotational flow, limiting the existence of large steady waves even for $U < U_{c1}$.

A main focus of the present work is to determine the dependence of this phenomenon on the vorticity and thickness of a linearly sheared liquid film. Therefore, an irrotational upper fluid of infinite extend is considered ($\zeta_2 = 0$, $y = 0$) and the critical current velocity correct to second order, U_{c2}, is obtained by equating the two roots in (3.3). Upon setting for simplicity $\zeta_1 = \zeta$ and using the non-dimentionalization mentioned above, the following expression is obtained:

$$U_{c2} = u_d \pm \left\{ \left(\frac{1+x}{1-x} + r \right) \Big/ \left[(1-r) + \frac{1-x}{1+x}\frac{\zeta^2}{4} + a^2 \Delta \right] \left(r \frac{1+x}{1-x} \right) \right\}^{\frac{1}{2}}, \tag{5.1}$$

where u_d is the liquid velocity defined by (2.10) and

$$\Delta = \frac{1}{2}\left(\lambda^2 \frac{1+x}{1-x} + r\lambda'^2 \right) - 2\lambda^2 \frac{(1+x)x}{(1-x)^3} - \frac{\zeta^2}{4}\frac{1+x^2}{1-x^2} + 2\lambda\zeta$$
$$\times \frac{x}{(1-x)^2} + \frac{1}{2} \frac{\left(\lambda^2 \dfrac{1+4x+x^2}{(1-x)^2} - r\lambda'^2 - 2\lambda\zeta \dfrac{1+x^2+x}{1-x^2} + \dfrac{\zeta^2}{2} \right)^2}{\lambda^2 \dfrac{1-x}{1+x} + r\lambda'^2}. \tag{5.2}$$

Again, only the positive root of (5.1) need to be considered. Using (2.11) for the linear velocity U_{c1}, equation (5.2) can be reformulated to read

$$(U_{c2} - u_d) = (U_{c1} - u_d) \left[1 + a^2 \frac{\Delta}{(1-r) + \dfrac{\zeta^2}{4}\dfrac{1-x}{1+x}} \right]^{\frac{1}{2}}, \tag{5.3}$$

which in the limit $\zeta = 0$ agrees with the expression given by Bontozoglou & Hanratty (1988). It is readily seen from (5.3) that $[(U_{c2}-u_d)^2/(U_{c1}-u_d)^2 - 1]$ varies linearly with the square of the wave amplitude, a^2, with the slope of the line dictating whether U_c is a decreasing or increasing function of a. A representative plot is shown in figure 3, where it is seen that vorticity may have a significant effect.

The slope of the dynamical limit line as a function of $\exp(-d_1)$ is shown in figure 4(a, b) for five values of constant vorticity, including the irrotational case, and for density ratios $r = 0.001$ and 0.1 (representative of gas/liquid flows under low and high pressure). It is interesting to note that regions with negative slope still exist and large values of vorticity cause the transition to a negative slope for a thicker liquid layer. The abrupt decrease in the value of the slope for very thin films is seen to take place for both positive and negative vorticities. The effect of vorticity is more evident for $r = 0.1$ and it is seen to be non-monotonic. Indeed, for deep liquid layers the dynamical limit slope is an increasing function of the vorticity value. On the other hand, in the limit $d_1 \to 0$, the slope tends to become a decreasing function of the absolute value of vorticity (irrespective of sign).

The above observations are reconfirmed by numerical computations, which indicate that the exact values of U_c compare well with the weakly nonlinear approximation for small to intermediate amplitudes.

5.2. *Numerical results*

The computational results presented in this section cover a region of the five-parameter space under investigation. Prominent parameters are the vorticity ζ of the lower layer

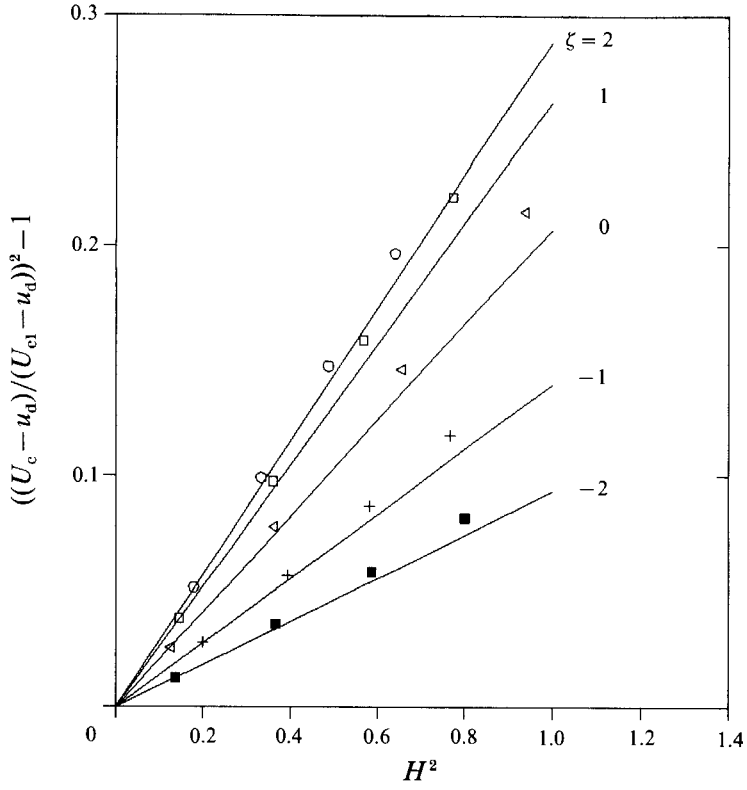

FIGURE 5. Critical current U_c as a function of wave height H for density ratio $r = 0.1$, $\exp(-d_1) = 0.25$ and various vorticities ζ. Straight lines represent the weakly nonlinear approximation and discrete points the fully nonlinear solution: ○, $\zeta = 2$; □ $\zeta = 1$; ◁, $\zeta = 0$, +, $\zeta = -1$; ■, $\zeta = -2$.

Vorticity ζ	Depth d	Phase velocity	Wave height: Present work – analytical results	Wave height: Present work – numerical results	Wave height: Teles da Silva & Peregrine (1988)
1	1	1.3580	0.5117	0.4998	0.50
1	1	1.4421	1.0905	0.9999	1.0
−1	1	0.5883	0.1175	0.1200	0.12
3	2	3.4440	1.0273	1.0000	1.0

TABLE 1. Comparison of results for surface waves

which varies from -2 to $+2$ (the upper layer is assumed to be irrotational), the current velocity U which varies from 0 to U_c, and the amplitude H which varies from 0 to the extreme value allowed by the numerical method implemented. The density ratio is taken equal to 0.0013 (typical value for air–water waves) and 0.1, while the parameter x which characterizes the depth of the lower layer varies from 0 to 1. The upper boundary is taken to the limit $y = 0$ ($d_2 \to \infty$).

The presented numerical results are based on a 64-point collocation scheme while the iteration procedure is considered to have converged when the residuals are less than 10^{-4}. In order to establish some confidence in the numerical results a comparison is made in table 1 with existing results for surface waves (Teles da Silva & Peregrine 1988). It is seen that the accuracy to expect from the code is satisfactory).

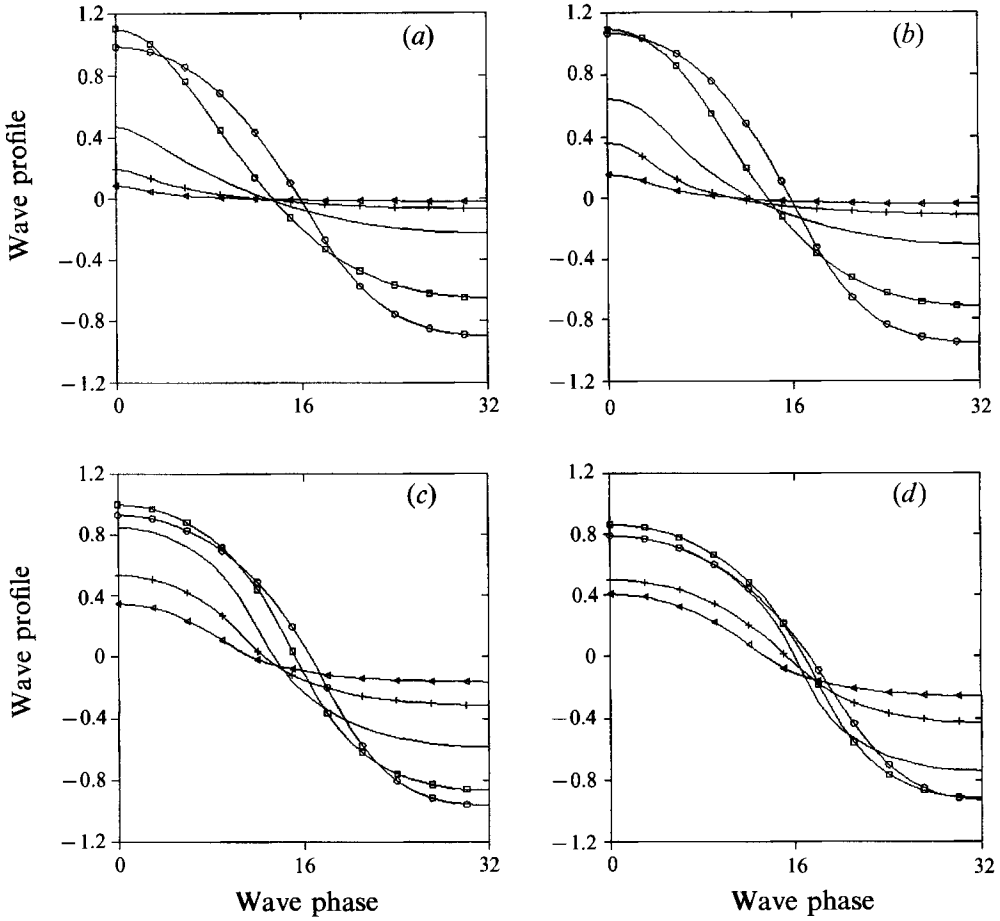

FIGURE 6. Profiles of high-amplitude waves for $r = 0.0013$, $\exp(-d_1) = 0.25$ and vorticities: ○, $\zeta = 2$; □, $\zeta = 1$; —, $\zeta = 0$; +, $\zeta = -1$; ◁, $\zeta = -2$. The current velocity is (*a*) $U = 0$, (*b*) $U = 10$, (*c*) $U = 20$, (*d*) $U = 25$.

The numerical results always compare well with the weakly nonlinear approximation for small and intermediate waves, for any density ratio and depth. This is demonstrated in figure 5 for the particular case of the critical current velocity, U_c, beyond which steady solutions cease to exist. The coordinates are such that the weakly nonlinear solutions are straight lines through the origin (see (5.3)). The agreement with the numerical results is excellent for small waves, while for higher waves the weakly nonlinear theory underestimates the critical current velocity compared to the fully nonlinear solution for any value of vorticity ζ.

Representative examples of the effect of positive and negative vorticity on the shape of the wave and the corresponding x-velocity component of the lower fluid at the interface of some high-amplitude air–water ($r = 0.0013$) waves are shown in figures 6 and 7 respectively. Since only waves symmetric about the crest are considered the wave profiles and velocities are plotted versus half the wave phase. The depth of the lower layer is $\exp(-d_1) = 0.25$ and the current velocity U is 0, 10, 20 and 25 in (*a*), (*b*), (*c*) and (*d*) respectively. In all figures the irrotational waves ($\zeta = 0$) are included to provide a direct comparison with the rotational waves of constant vorticity ($\zeta = \pm 1, \pm 2$).

It is seen from figure 6 that the presence of positive vorticity increases the amplitude

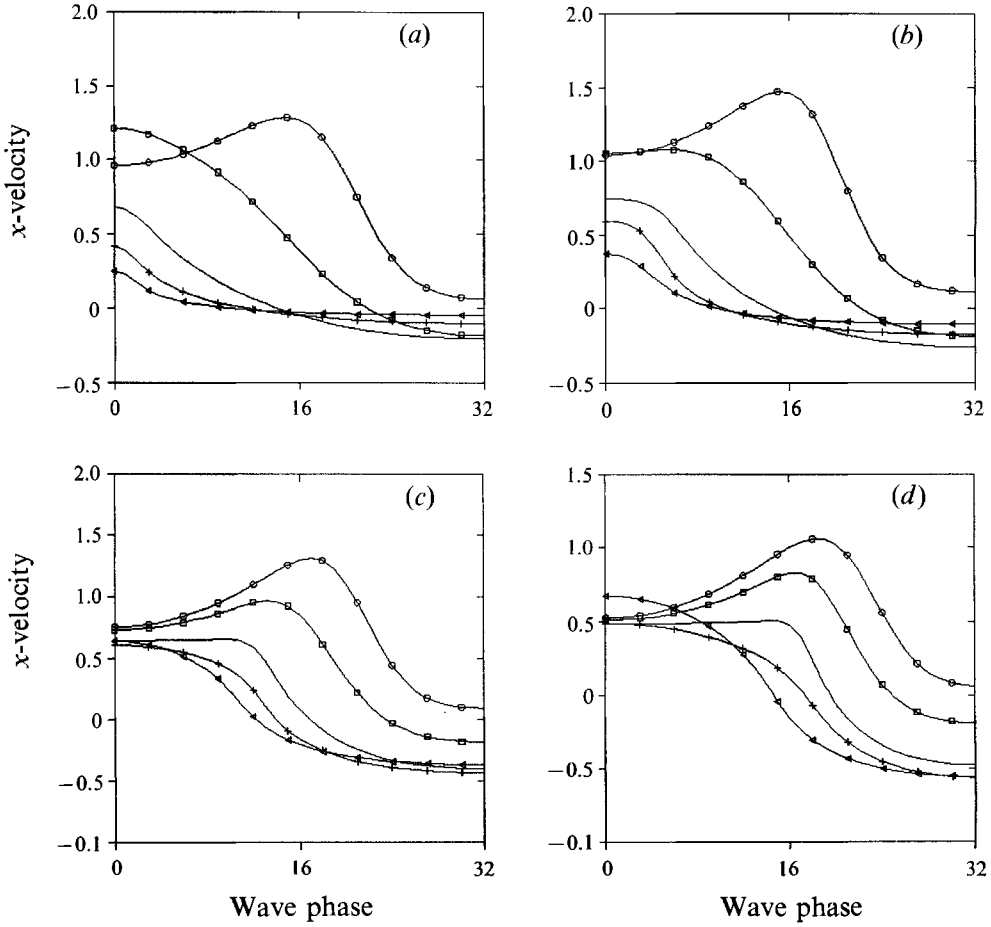

FIGURE 7. The x-velocity component of the lower fluid particles at the interface of the high-amplitude waves shown in figure 6 for $r = 0.0013$, $\exp(-d_1) = 0.25$ and vorticities: ○, $\zeta = 2$; □, $\zeta = 1$; —, $\zeta = 0$; +, $\zeta = -1$; ◁, $\zeta = -2$. The current velocity is (*a*) $U = 0$, (*b*) $U = 10$, (*c*) $U = 20$, (*d*) $U = 25$.

of the waves which become more rounded, while the presence of negative vorticity produces waves with smaller amplitudes and sharper crests. This result is clearer for small values of current velocities U, having been described for free-surface waves by Tsao (1959), Simmen & Saffman (1983) and Teles Da Silva & Peregrine (1988), while the effect of large current velocities U (close to U_c) on the shape of the waves seems to counterbalance the effect of vorticity.

The x-component of the velocity versus wave phase, shown in figure 7 in a physical reference frame, corresponds to the air–water waves shown in figure 6. Note that the large regions of almost constant horizontal velocity, which characterize interfacial irrotational waves with large current velocities U, disappear under the effect of vorticity. Now the point of a maximum x-velocity is clearly identified and for all cases with sufficiently large positive vorticity it is away from the crest even for small U (Stokes waves).

It is clear that the overall shape of the wave and the x-velocity component of the lower fluid at the interface are strongly affected by the vorticity ζ. It may be concluded that large values of positive vorticity allow the existence of high-amplitude waves with

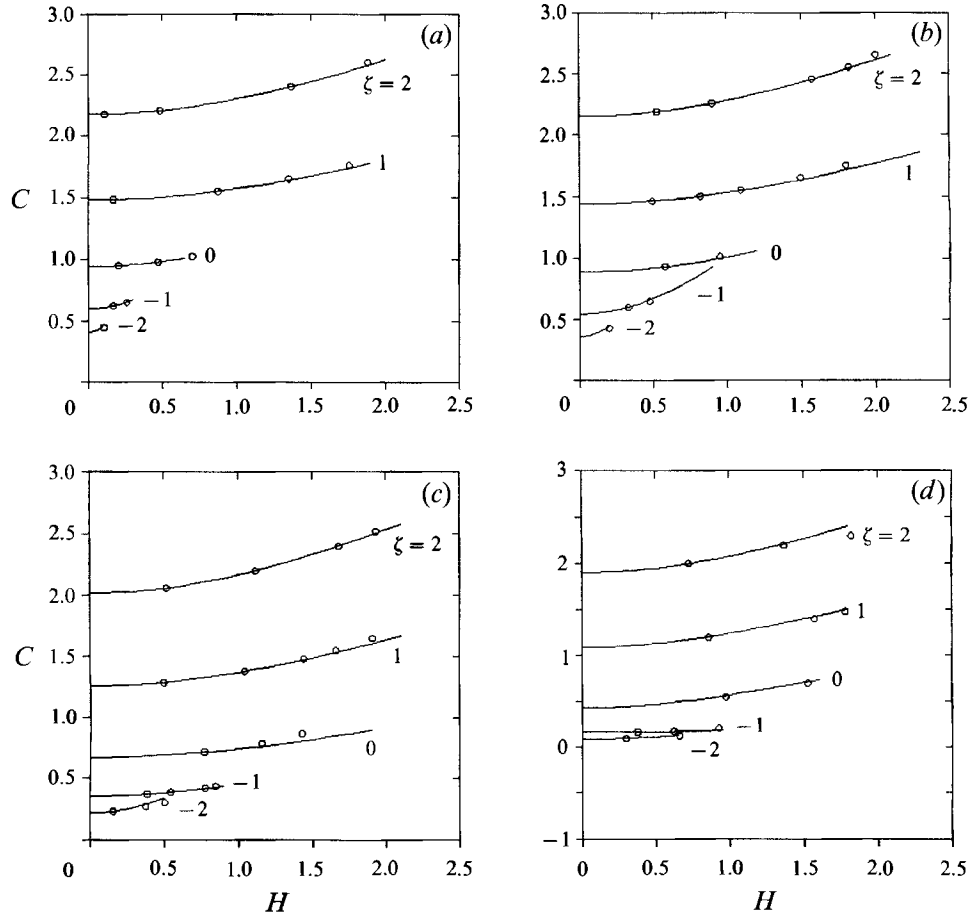

FIGURE 8. Wave celerity C as a function of the wave height H for $r = 0.0013$, $\exp(-d_1) = 0.25$ and various vorticities ζ. The current velocity is (*a*) $U = 0$, (*b*) $U = 10$, (*c*) $U = 20$, (*d*) $U = 25$. Curves represent the weakly nonlinear approximation and discrete points the fully nonlinear solution.

higher velocities. On the other hand the presence of negative vorticity, which corresponds to shear generated by the wind, favours the existence of waves of small amplitude with small velocities. This result holds for any U although it is more evident for small U. Similar results have been found for $\exp(-d_1) = 0.5$.

The phase velocities of waves for a wide range of vorticities for $\exp(-d_1) = 0.25$ are given in figure 8. Again the current velocity U is 0, 10, 20 and 25 in (*a*), (*b*), (*c*) and (*d*) respectively. As with rotational surface waves, phase velocities increase with amplitude for any U. However it is seen that for negative values of vorticity and large current velocities U the phase velocity becomes almost independent of H and equal to the linear phase speed of the wave. One of the implications of this result is that the iterative procedure becomes more vulnerable to numerical instabilities and may diverge. This behaviour becomes more evident when the depth of the lower layer decreases.

It is well known that, as the wave height increases, the x-velocity component at some point along the profile approaches the phase speed of the wave. Holyer (1979), extending Stokes limit for free-surface waves, considered the condition $u = C$ as a geometrical limit. However, Meiron & Saffman (1983) and Grimshaw & Pullin (1986) have demonstrated that S-shaped overhanging waves, although subject to Ray-

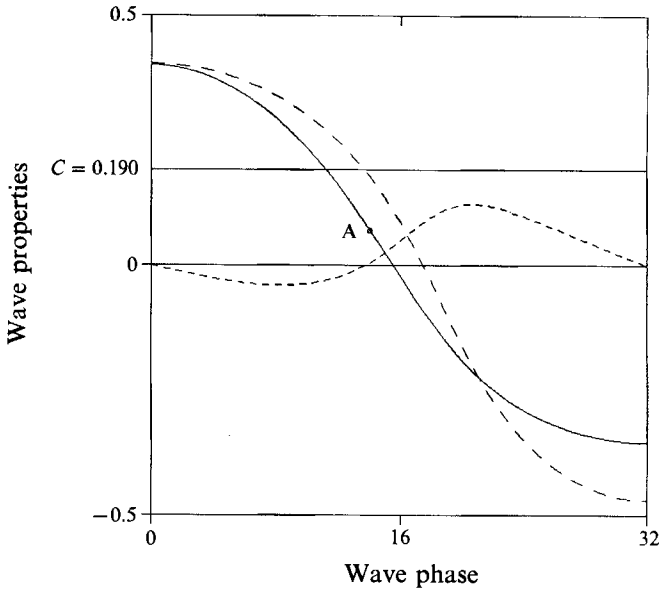

FIGURE 9. Wave profile and velocity components of the lower fluid at the interface for $H = 0.756$, $C = 0.190$, $U = 25$, $r = 0.0013$ and $\exp(-d_1) = 0.25$. ——, Wave profile; ——, x-velocity; ----, y-velocity.

leigh–Taylor instability, are steady solutions of the governing equations. Furthermore, regions with x-velocity higher than the phase speed are associated with these steady overhanging waves. Having all this in mind it is rather interesting to observe the horizontal and vertical velocity components of the lower fluid along the interface, shown in figure 9 in a physical reference frame for $H = 0.756$, $C = 0.190$, $U = 25$, $r = 0.0013$, $\zeta = -1$, and $\exp(-d_1) = 0.25$. It is readily observed that the value of the x-velocity component at the wave crest is larger than the phase speed C and it drops to C at some point A, while the wave profile does not have an infinite slope at this point or anywhere else. This discrepancy is clarified by noticing that the y-velocity component goes through zero at this point A and then changes sign as the crest is approached. Point A, therefore, is a stagnation point in the reference frame where the wave is stationary, as is its symmetric counterpart relative to the wave crest.

This result is a first indication of a new flow structure consisting of a recirculating eddy at the wave crest. A detailed description of this is given in the next section.

6. High-amplitude waves with separated flow

The aforementioned flow structure, which, in a stationary reference frame includes two stagnation points on the interface and contains a recirculating eddy at the crest, has been repeatedly encountered for negative values of vorticity in the present work. For fixed values of the parameters r, U, d_1 and ζ ($\zeta < 0$), it appears only above a certain wave amplitude. Representative velocity fields are shown in figure 10 for air–water ($r = 0.0013$) waves with $U = 25$ and $\exp(-d_1) = 0.25$. In this case a stagnation point is first observed at the crest at a wave height $H = 0.302$ and then expands with increasing amplitude to generate a closed eddy.

The wave height at which the recirculating eddy first appears, for a given density ratio and depth, is a function of the current velocity and the vorticity of the liquid layer.

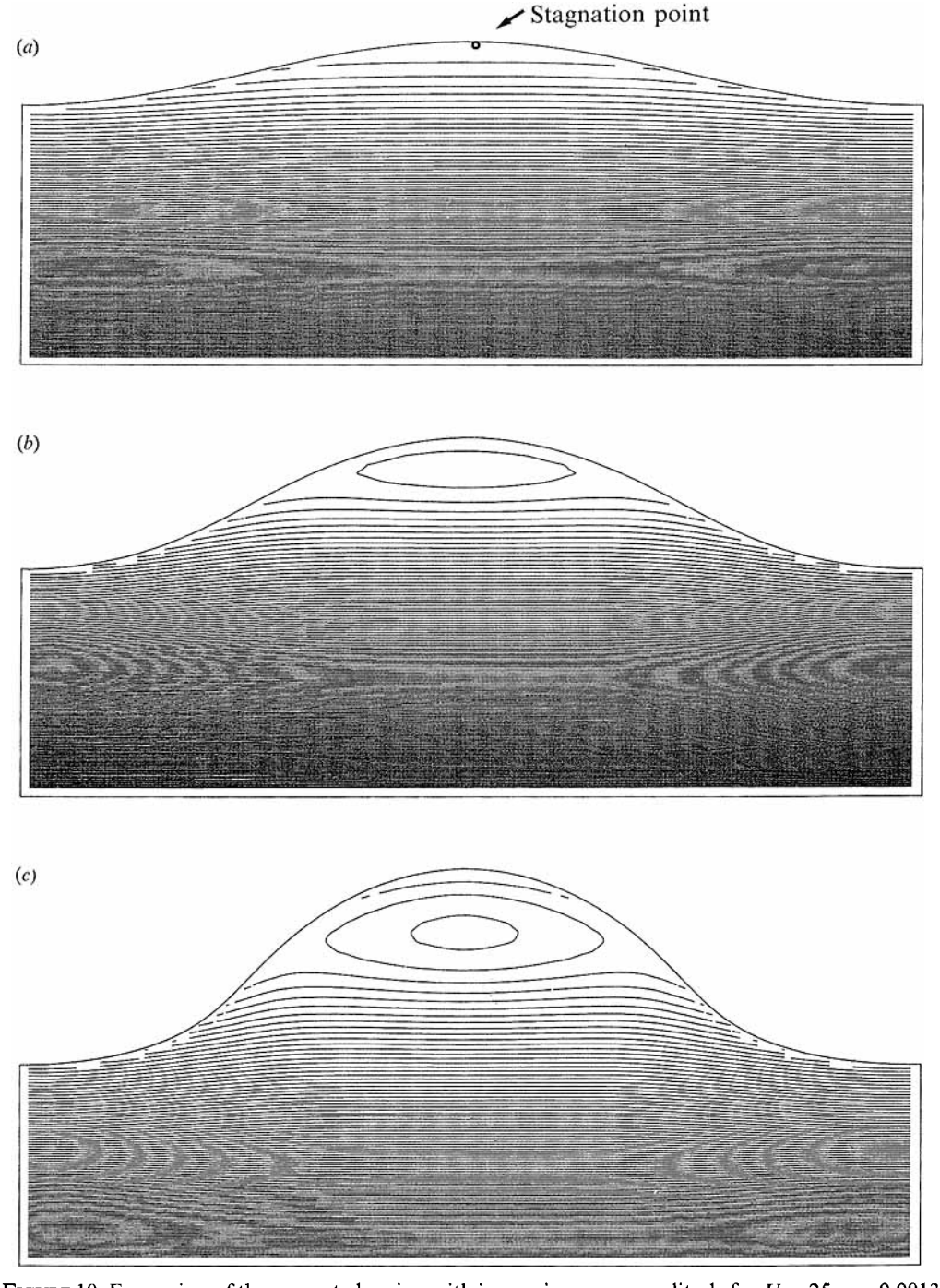

FIGURE 10. Expansion of the separated region with increasing wave amplitude for $U = 25$, $r = 0.0013$, $\zeta = -1$ and $\exp(-d_1) = 0.25$. (*a*) $H = 0.302$, $C = 0.168$, (*b*) $H = 0.620$, $C = 0.180$, (*c*) $H = 0.924$, $C = 0.210$.

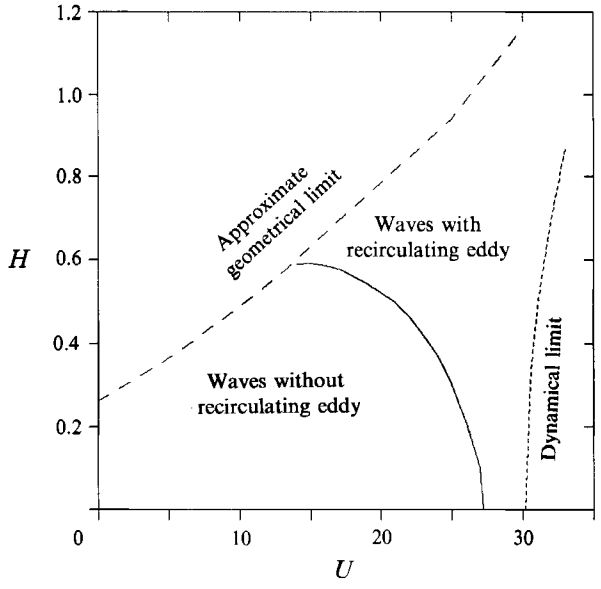

FIGURE 11. Sketch of wave solution domain with and without an eddy at the crest for $r = 0.0013$, $\zeta = -1$ and $\exp(-d_1) = 0.25$.

The solid line in figure 11 shows the boundary in the (H, U) solution domain between waves with and without an eddy at the crest for $r = 0.0013$, $\zeta = -1$ and $\exp(-d_1) = 0.25$. The region comprising waves with separated flow is above this boundary and is bounded from the right by the dynamical limit which appears in the figure and from the top by the geometrically limiting highest waves, which have not been rigorously calculated in the present work. It is readily observed from figure 11 that the higher the current velocity U, the earlier the separation occurs. It can also be inferred from figure 11 that separation eddies should not be observed below a certain current velocity. This fact explains why such eddies have not been reported for surface waves by Simmen & Saffman (1985) and Teles Da Silva & Peregrine (1988). In this sense, the closed eddy at the wave crest can be considered as an effect of the wind. Representative calculations with $\zeta = -2$, and $\exp(-d_1) = 0.5$ indicate that increasing the absolute value of the vorticity or decreasing the depth of the lower fluid leads to the appearance of the separation eddy at lower wave amplitudes.

One particular observation from figure 11 is that all waves, above a current velocity roughly equal to $U = 28$, comprise a separation eddy. Velocity fields for different wave heights are shown for such a case in figure 12 with $U = 30$, $\zeta = -1$ and $\exp(-d_1) = 0.25$. From figure 12 it can be observed that, for the smaller amplitude, the separated region consists of an elongated eddy containing almost the entire liquid volume above the level of the trough. With increasing wave height, the separation eddy approaches a more rounded shape but still covers the major part of the wave crest. An interesting consequence is that the distortion in the flow field caused by the wavy interface is, with the appearance of this prominent separated region, largely confined to the crest of the wave. Indeed, the flow field below the upper part of the wave is almost identical to the base flow. Evidently this is not the case for relatively large wave heights in the absence of the recirculating eddy.

The onset of flow separation can be understood as a straightforward consequence of the constant-vorticity model, by the following simple arguments. Figure 1(*a*, *b*)

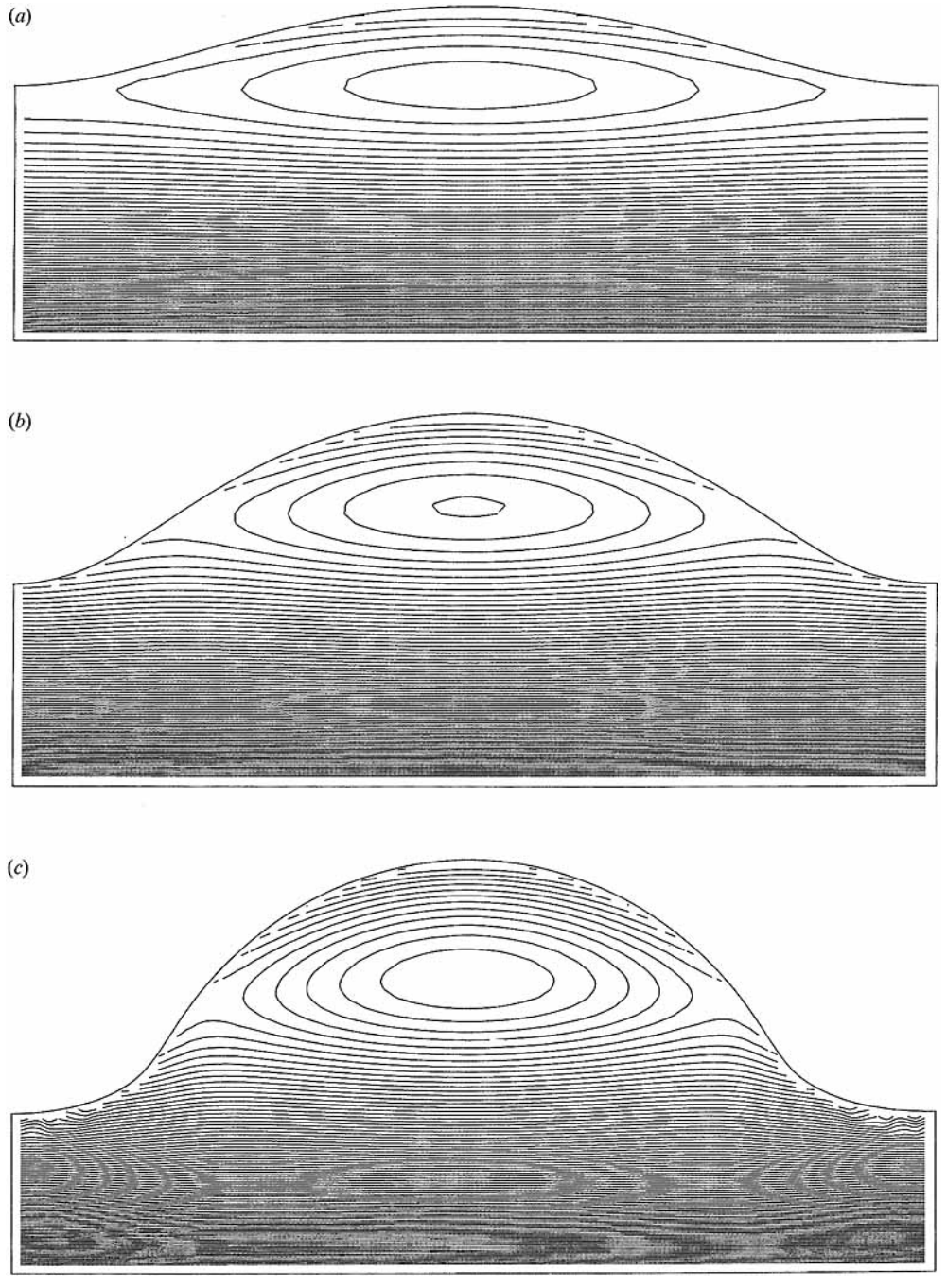

FIGURE 12. Streamlines of lower fluid for $U = 30$, $r = 0.0013$, $\zeta = -1$, $\exp(-d_1) = 0.25$ and different wave heights. (*a*) $H = 0.368$, $C = -0.210$, (*b*) $H = 0.786$, $C = -0.110$, (*c*) $H = 1.166$, $C = -0.035$.

represents the shear profile for two cases, one with negative and one with positive vorticity. Two reference frames are depicted, the one to the right corresponding to a wave stationary on a stream. It is seen that, for positive phase velocity C, a critical layer in the classical sense of linear stability, can only occur for positive vorticity (figure 1*b*).

This setup has been considered by Teles da Silva & Peregrine (1988) for free surface waves. They further point out that, with a critical layer, 'cat's eye' eddies form for any finite-amplitude wave.

The situation is more interesting when a critical layer forms above the mean water level and, therefore, does not manifest itself unless the waves reach a certain height. This is possible for flow with negative vorticity, as shown in figure 1(*a*). It is believed that this occurrence is the generating mechanism for the separation eddies in figure 10 and, further, dictates the extend of the separation region. It is also noted that, for current velocities U near the limiting value, the phase speed of the waves becomes negative and the critical layer occurs slightly below the mean level. This situation produces the extended separation eddies depicted in figure 12. The above simplified arguments do not consider the straining imposed by the irrotational wave motion, which is taken into account in the present numerical computations.

7. Concluding remarks

Interfacial, gravity waves of permanent form are calculated – both analytically and numerically – in a configuration involving a lower fluid with constant vorticity, bounded by an upper fluid in uniform motion.

The dynamical limit to the existence of steady solutions is calculated and the effect of non-zero vorticity appears to be significant. In particular, previous observations about the slope of the curve of the critical current velocity versus wave amplitude turning from positive to negative for very thin films (Bontozoglou & Hanratty 1988) are shown to hold for deeper films in the presence of non-zero vorticity.

It is recalled that the existence/non-existence of steady solutions at current velocities above the critical linear is associated with supercritical stability/subcritical instability (Miles 1986). In this light, the transition of the dynamical limit slope from positive to negative can be taken to signify a change in the behaviour of linearly unstable disturbances on such thin films. In particular, a positive slope is argued to indicate that the fundamental harmonic remains dominant and finite-amplitude gravity waves will actually be observed. On the other hand, a negative slope of the dynamical limit line indicates that during nonlinear evolution all superharmonics are simultaneously excited (Drazin & Reid 1981), leading to a pebbly interface with no observable gravity wave. These inferences are in accordance with experimental observations (Andreussi, Asaly & Hanratty 1985), which indicate that roll waves do not appear on very thin films, even when they are sheared by gas flows well above the linear stability limit.

The effect of positive and negative vorticity on the wave profile and on the velocity field of the lower fluid in the presence of a current velocity is demonstrated in the present work. An unexpected flow structure, involving a closed eddy on the wave crest, is calculated for the case of negative vorticity and high enough wave amplitude. Its earlier manifestation, where the separation region shrinks to a point, corresponds to a stagnation point in the steady flow, right on the crest of the wave.

This configuration has been considered to be the onset of incipient breaking (Banner & Phillips 1974) in the similar situation of a drift current on top of an irrotational mass of water. The present work provides numerical evidence for the existence of progressive waves of permanent form beyond the point of incipient breaking. Thus, it is an example where the conjecture of Banner & Phillips (1974) that 'if the flow is rotational there is no necessity for the stagnation point at the crest to be associated with a discontinuity in surface slope' (i.e. a geometrical singularity) holds true. It should be remembered, however, that in the actual configuration considered by the above authors, Miche

(1944) shows that a stagnation point at the crest is always associated with a 120° angle. Thus, the recirculating eddy at the wave crest can be considered as an effect of the wind.

The present problem differs from the one posed by Banner & Phillips (1974) in that the constant-vorticity region extends throughout the entire lower fluid. Therefore, it more closely represents shallow-water waves breaking under the action of wind. These are frequently described in the experimental literature as roll waves, from the distinctive appearance of the crest region which seems to constantly roll over itself.

The ability of the inviscid, rotational theory to provide steady wave solutions beyond incipient breaking is interesting from a fundamental standpoint. The crucial question, however, remains of whether these solutions are a realistic representation of actual roll waves. This issue is not pursued any further in the present work and remains to be investigated. It is only noted that there is an encouraging qualitative resemblance with actual waves, in that closed eddies appear only above a current velocity. Furthermore, the picture of the crest eddy – rolling on a substrate whose flow field is close to the basic flow – which emanates from the present computations, is similar to experimentally observed roll waves on highly sheared thin films (Hanratty 1983).

Finally, it is noted that some of the parameters considered here, though formally independent as far as inviscid theory is concerned, are actually related in real flows. For example if the shear is generated by the gas flow, ζ and U depend on each other and realistic estimates can be made by considering a turbulent velocity profile in the gas and calculating the shear stress exerted on the flat liquid surface. Such considerations will be pursued in future work and will help in viewing the theoretical results from a more applied perspective.

Appendix

The dispersion relation (3.3) is derived by substituting the leading-order terms for the wave profile

$$\eta(w) = a\cos w + a_2\cos 2w, \tag{A 1}$$

and the velocity potentials

$$\phi_1(x,y,t) = A_1(\mathrm{e}^{ky}+\mathrm{e}^{-2kd_1}\mathrm{e}^{-ky})\sin w + \tfrac{1}{2}A_2(\mathrm{e}^{2ky}+\mathrm{e}^{-4kd_1}\mathrm{e}^{-2ky})\sin 2w \tag{A 2}$$

and

$$\phi_2(x,y,t) = Ux + B_1(\mathrm{e}^{ky}+\mathrm{e}^{2kd_2}\mathrm{e}^{-ky})\sin w + \tfrac{1}{2}B_2(\mathrm{e}^{2ky}+\mathrm{e}^{4kd_2}\mathrm{e}^{-2ky})\sin 2w, \tag{A 3}$$

into expression (3.2). In the above expansions a is half the wave height ($H = 2a$) and $w = kx - \omega t$ is the wave phase. Next, taking the partial derivatives of the resulting expression with respect to coefficients A_1, A_2, B_1, B_2 and a_2 yields

$$A_1 = \lambda a/(1-x), \tag{A 4}$$

$$B_1 = -\lambda' a/(1-y^{-1}), \tag{A 5}$$

$$A_2 = 2\frac{\lambda}{k}\frac{ka_2(1+x^2)+\frac{1}{2}k^2a^2(1-x^2)}{(1-x^4)}+\tfrac{1}{2}\zeta_1\frac{a^2}{1-x^2}-2k\lambda a^2\frac{(1+x^3)(1+x)}{(1-x^4)(1-x^2)}, \tag{A 6}$$

$$B_2 = -2\frac{\lambda'}{k}\frac{ka_2(1+y^{-2})+\frac{1}{2}k^2a^2(1-y^{-2})}{1-y^{-4}}+\tfrac{1}{2}\zeta_2\frac{a^2}{1-y^{-2}}+2k\lambda' a^2\frac{(1+y^{-3})(1+y^{-1})}{(1-y^{-4})(1-y^{-2})} \tag{A 7}$$

and

$$a_2 = \tfrac{1}{2}a^2 \times \left[\frac{k^2\left[\lambda^2\frac{1+4x+x^2}{(1-x)^2}-r\lambda'^2\frac{1+4y+y^2}{(1-y)^2}\right]-2k\left[\lambda\zeta_1\frac{1+x^2+x}{1-x^2}-r\lambda'\zeta_2\frac{1+y^2+y}{1-y^2}\right]+\frac{1}{2}(\zeta_1^2-r\zeta_2^2)}{-[g(1-r)+\lambda\zeta_1+r\lambda'\zeta_2]+2k\left[\lambda^2\frac{1+x^2}{1-x^2}+r\lambda'^2\frac{1+y^2}{1-y^2}\right]}\right]. \tag{A 8}$$

Finally, substituting the above coefficients back into the Lagrangian (3.2), and after some algebraic manipulations of the resulting equation, the second-order dispersion relation (3.3) is obtained.

REFERENCES

ANDREUSSI, P., ASALI, J. C. & HANRATTY, T. J. 1985 Initiation of roll waves in gas–liquid flows. *AIChE J.* **31**, 119.

BANNER, M. L. & PHILLIPS, O. M. 1974 On the incipient breaking of small scale waves. *J. Fluid Mech.* **65**, 647.

BATEMAN, H. 1944 *Partial Differential Equations*. Cambridge University Press.

BONTOZOGLOU, V. & HANRATTY, T. J. 1988 Effects of finite depth and current velocity on large amplitude Kelvin–Helmholtz waves. *J. Fluid Mech.* **196**, 187.

DRAZIN, P. G. 1970 Kelvin–Helmholtz instability of finite amplitude. *J. Fluid Mech.* **42**, 321.

DRAZIN, P. G. & REID, W. H. 1981 *Hydrodynamic Stability*. Cambridge University Press.

GRIMSHAW, R. H. J. & PULLIN, D. I. 1986 Extreme interfacial waves. *Phys. Fluids* **29**, 2802.

HANRATTY, T. J. 1983 Interfacial instabilities caused by the air flow over a thin liquid layer. In *Waves on Fluid Interfaces* (ed. R. E. Meyer), p. 221. Academic.

HOLYER, J. Y. 1979 Large amplitude progressive interfacial waves. *J. Fluid Mech.* **93**, 433.

LONGUET-HIGGINS, M. S. & COKELET, E. D. 1976 The deformation of steep surface waves on water. A numerical method of computation. *Proc. R. Soc. Lond.* A **350**, 1.

LUKE, J. C. 1967 A variational principle for a fluid with a free surface. *J. Fluid Mech.* **27**, 395.

MASLOWE, S. A. & KELLY, R. E. 1970 Finite amplitude oscillations in a Kelvin–Helmholtz flow. *Intl J. Non-linear Mech.* **5**, 427.

MEIRON, D. J. & SAFFMAN, P. G. 1983 Overhanging gravity waves of large amplitude. *J. Fluid Mech.* **129**, 213.

MICHE, M. 1944 Mouvements ondulatoires de la mer en profondeur constante ou decroissant. *Ann. Ponts Chaussees* **114**, 374.

MILES, J. W. 1986 Weakly nonlinear Kelvin–Helmholtz waves. *J. Fluid Mech.* **172**, 513.

MILINAZZO, F. A. & SAFFMAN, P. G. 1990 Effect of a surface shear layer on gravity and gravity–capillary waves of permanent form. *J. Fluid Mech.* **216**, 93.

NAYFEH, A. H. & SARIC, W. S. 1972 Nonlinear waves in a Kelvin–Helmholtz flow. *J. Fluid Mech.* **55**, 311.

NEW, A. L., MCIVER, P. & PEREGRINE, D. H. 1985 Computations of overturning waves. *J. Fluid Mech.* **150**, 233.

PULLIN, D. I. & GRIMSHAW, R. H. J. 1983 Interfacial progressive gravity waves in a two-layer shear flow. *Phys. Fluids* **26**, 1731.

PULLIN, D. I. & GRIMSHAW, R. H. J. 1986 Stability of finite-amplitude interfacial waves. Part 3. The effect of basic current shear for one-dimensional instabilities. *J. Fluid Mech.* **172**, 277.

SAFFMAN, P. G. & YUEN, H. C. 1982 Finite-amplitude interfacial waves in the presence of a current. *J. Fluid Mech.* **123**, 459.

SIMMEN, J. A. & SAFFMAN, P. G. 1985 Steady deep-water waves on a linear shear current. *Stud. Appl. Maths* **73**, 35.

TELES DA SILVA, A. F. & PEREGRINE, D. H. 1988 Steep, steady surface waves on water of finite depth with constant vorticity. *J. Fluid Mech.* **195**, 281.

TSAO, S. 1959 Behavior of surface waves on a linearly varying current. *Mosk. Fiz. Tekh. Inst. Issled. Mekh. Prikl. Mat.* **3**, 66.

WHITHAM, G. B. 1974 *Linear and Nonlinear Waves*. Wiley-Interscience.